

# Magnetic ordering in the striped nickelate $\text{La}_{5/3}\text{Sr}_{1/3}\text{NiO}_4$ : A band structure point of view

UDO SCHWINGENSCHLÖGL<sup>1</sup>, COSIMA SCHUSTER<sup>1</sup> and RAYMOND FRÉSARD<sup>2</sup>

<sup>1</sup> *TP II, Institut für Physik, Universität Augsburg, D-86135 Augsburg, Germany*

<sup>2</sup> *Laboratoire CRISMAT, UMR CNRS-ENSICAEN(ISMRA) 6508, 6 Bld. du Maréchal Juin, F-14050 Caen, France*

PACS 71.20.-b – Electron density of states and band structure of crystalline solids  
PACS 71.45.Lr – Charge-density-wave systems  
PACS 75.25.+z – Spin arrangements in magnetically ordered materials

**Abstract.** - We report on a comprehensive study of the electronic and magnetic structure of the striped nickelate  $\text{La}_{5/3}\text{Sr}_{1/3}\text{NiO}_4$ . The investigation is carried out using band structure calculations based on density functional theory. A magnetic structure compatible with experiment is obtained from spin-polarized calculations within the generalized gradient approximation (GGA), whereas inclusion of a local Coulomb interaction in the LDA+ $U$  framework results in a different ground state. The influence of the various interaction parameters is discussed in detail.

Stripe phases are currently the focus of an intense activity as they are observed in a wealth of systems. Most of them are layered oxides, including cuprates [1–4], nickelates [5–9], and manganites [10–12]. In such doped Mott insulators the structure of these phases varies from system to system: the domain walls in which the holes are primarily located can run parallel to the lattice axes, or along the diagonal. Furthermore, the distance between them is either compatible with one doped hole per two domain walls, in the so-called *half-filled stripes*, or with one doped hole per one domain wall in the *filled stripes*, as discussed by Zaanen and Oleś [13]. Those various structures are realized in different systems, e. g., half-filled vertical stripes in the lightly doped cuprate  $\text{Ca}_{1.88}\text{Na}_{0.12}\text{CuO}_2\text{Cl}_2$ , and diagonal filled stripes in  $\text{La}_{2-x}\text{Sr}_x\text{NiO}_4$ . Stripe formation manifests itself in a wealth of experiments, in particular by the appearance of peaks in both unpolarized and polarized neutron scattering experiments. Indeed charge and spin order in  $\text{La}_{2-x}\text{Sr}_x\text{NiO}_4$  is characterized by the wave vectors  $\mathbf{Q}_c = 2\pi(\epsilon, \epsilon)$  and  $\mathbf{Q}_s = \pi(1 \pm \epsilon, 1 \pm \epsilon)$ , respectively, with  $\epsilon \simeq x$  corresponding to a constant charge density of one hole/Ni ion along the diagonal stripe. Incidentally, the electronic states involved in the stabilization of the stripe phases form *mid-gap* bands; in the first case these bands are partially filled, sometimes even half-filled, while in the second case these bands are filled (for a recent discussion see Ref. [14]). From the point of view of describing these phases by means of microscopic models it is commonly accepted that the one band Hubbard model is suitable for

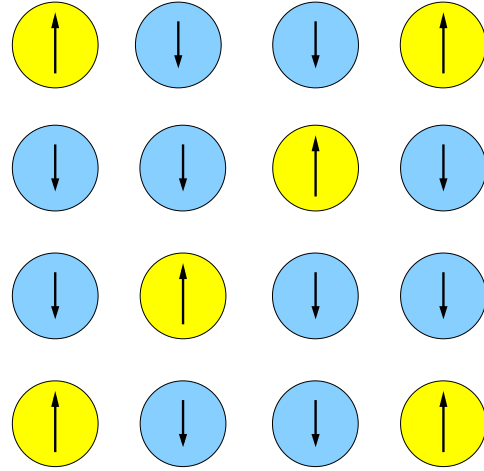


Fig. 1: (Color online) Magnetic structure of the Ni atoms in the NiO-planes of  $\text{La}_{5/3}\text{Sr}_{1/3}\text{NiO}_4$ . Bright (yellow) circles correspond to Ni1/Ni2 sites, dark (blue) circles to Ni3/Ni4 sites. The representation refers to the experimental CDFAS phase, see the text for details.

the cuprates, whereas the orbital degeneracy incorporated in a two-band Hubbard Hamiltonian plays a prominent role when studying nickelates. In both cases it turns out that the parameters of the model deeply influence the type of ground state (see, e. g., Ref. [15]), and it would be desirable to obtain an estimate of them from *ab initio* cal-

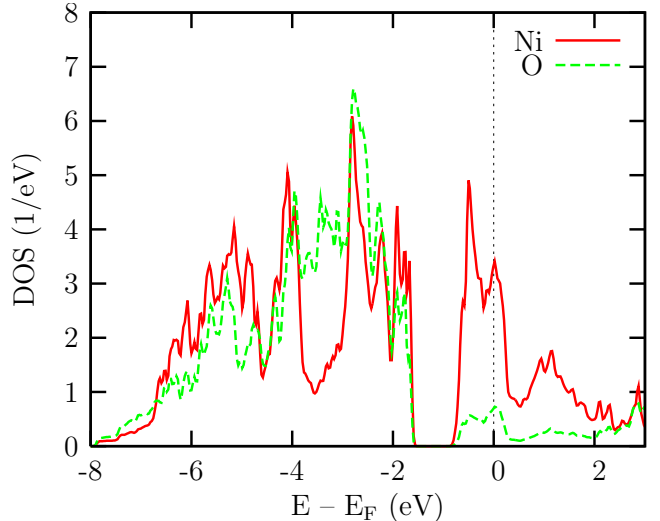
arXiv:0711.1599v1 [cond-mat.str-el] 10 Nov 2007

	semi-core states	valence states
Sr	4s, 4p	5s, 5p
Ni	3p	3d, 4s, 4p
La	5s, 5p	4f, 5d, 6s, 6p
O	2s	2p, 3s

Table 1: Choice of semi-core and valence states.

culations. Indeed, when comparing a doubly degenerate Hubbard model to a more realistic Hamiltonian containing  $e_g$  states [16], the former predicts bond centered diagonal half-filled stripes to be the ground state, whereas diagonal filled stripes are promoted in the latter case. Besides, the relevance of the Jahn-Teller coupling was emphasized by Zaanen and Littlewood [17]. Therefore a band structure calculation embracing all these aspects is expected to provide insight into the mechanism leading to the stripe formation. As compared to the cuprates, quantum fluctuations should play a smaller role in the nickelates where the  $\text{Ni}^{2+}$  ions carry spin 1. The approximations involved in the band structure calculations hence are expected to have less impact. In this work we focus on the doping  $x = 1/3$ , where the wave vectors characterizing spin and charge modulations coincide as  $Q_{s,c} = \frac{\pi}{3}(1, 1)$ . This case corresponds to the most stable stripe phase with an ordering temperature of  $T \sim 240$  K, as revealed by specific heat [18], transport [19], and optical conductivity data [20]. For a more comprehensive review of the experimental situation we refer to Ref. [16].

The crystal structure of the  $\text{La}_{2-x}\text{Sr}_x\text{NiO}_4$  compounds is based on the body-centered tetragonal  $\text{K}_2\text{NiF}_4$  structure with space group  $I4/mmm$  [21], as for the  $\text{La}_{2-x}\text{Sr}_x\text{CuO}_4$  system [22]. Therefore, the tetragonal unit cell comprises two  $\text{La}_{2-x}\text{Sr}_x\text{NiO}_4$  formula units. The compounds essentially consist of  $\text{NiO}_6$  octahedra forming layers parallel to the  $ab$ -plane, where neighbouring layers are separated by La/Sr ions. To be more specific, the magnetic Ni atoms are arranged on a square planar lattice and interact via the O atoms located midway between them. By symmetry, there are two crystallographically inequivalent NiO planes, which, however, are closely related to each other. We have obtained the structural parameters for our band structure calculations by interpolation between the experimental values at compositions of  $x = 0$  and  $x = 0.6$ . For the composition of interest,  $x = 1/3$ , the lattice constants amount to  $a = 3.83$  Å and  $c = 12.68$  Å. While the La/Sr sites are located at (4e) Wyckoff positions with parameter  $z = 0.3617$ , the Ni and O(1) sites occupy (2e) and (4c) Wyckoff positions, respectively. Finally, for the O(2) sites we again have to deal with (4e) Wyckoff positions, where the parameter is  $z = 0.174$ . In order to account for the realized spin and charge modulations, we set up a supercell of the tetragonal unit cell. Comprising altogether six  $\text{La}_{5/3}\text{Sr}_{1/3}\text{NiO}_4$  formula units with 12 La/Sr sites, our supercell is given by the lattice vectors (1, 1, 0), (3, 0, 0), and (0, 0, 1), with respect to the tetragonal lattice. In order to

Fig. 2: (Color online) Partial Ni 3d and O 2p DOS (per unit cell) for spin-degenerate  $\text{La}_{5/3}\text{Sr}_{1/3}\text{NiO}_4$ , as obtained by the LDA+ $U$  method.

satisfy the La:Sr ratio of 5:1, we have to attribute 10 La and 2 Sr atoms to the 12 La/Sr sites, where the details of the distribution do not affect our further argumentation. As a consequence, we have four classes of inequivalent Ni sites, called Ni1, Ni2, Ni3, and Ni4 in the following. Sites Ni1 and Ni3 are located in one of the inequivalent NiO planes, while sites Ni2 and Ni4, respectively, correspond to them in the other NiO plane. The positions of sites Ni1 and Ni3 are translated into that of Ni2 and Ni4, respectively, by the vector  $(a/2, a/2, c/2)$ . The charge and spin pattern covered by these structural prerequisites is illustrated in fig. 1. We have diagonal stripes of Ni1 (Ni2) sites, separated by domains of Ni3 (Ni4) sites, thus reflecting the coincidence of the spin and charge wave vectors.

The electronic structure calculations presented in the following rely on density functional theory (DFT). Concerning the DFT implementation, we apply the Wien2k package, a state-of-the-art full-potential code with mixed lapw and apw+lo basis set [23]. This code has shown great capacity in dealing with the interplay of structural relaxation, magnetic interaction and electronic correlations in very complex materials [24]. In each of our calculations, the charge density is represented by almost 23,000 plane waves and the mesh for the Brillouin zone integration comprises 60  $\mathbf{k}$ -points in the irreducible wedge. Our choice of semi-core and valence states is summarized in table 1. For the supercell setup described above, we address calculations within the pure generalized gradient approximation (GGA) as well as LDA+ $U$  calculations to account for an additional local electron-electron interaction. We use the Perdew-Burke-Ernzerhof [25] parameterization of the exchange-correlation functional for the pure GGA, while the LDA+ $U$  calculations are based on the SIC scheme described in [26, 27]. In each case, we use a band structure calculation where we artificially enforce spin-degeneracy as

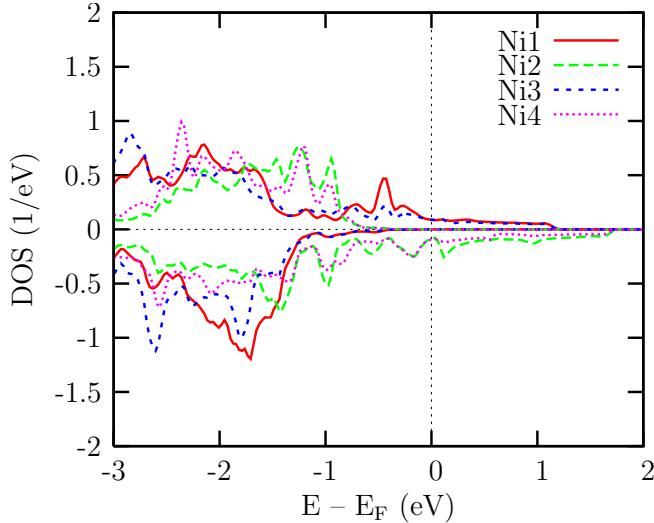


Fig. 3: (Color online) Partial spin-majority and spin-minority Ni 3d DOS (per Ni atom) for spin-polarized  $\text{La}_{5/3}\text{Sr}_{1/3}\text{NiO}_4$  in the ADFAS phase, as obtained by the LDA+ $U$  method.

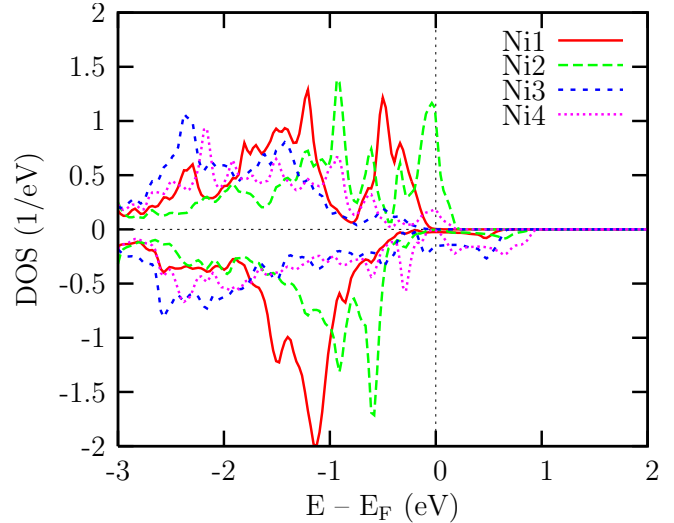


Fig. 4: (Color online) Partial spin-majority and spin-minority Ni 3d DOS (per Ni atom) for spin-polarized  $\text{La}_{5/3}\text{Sr}_{1/3}\text{NiO}_4$  in the CDFAS phase, as obtained by the LDA+ $U$  method.

reference for the total energy gain of specific spin patterns. In particular, we investigate diagonal filled ferromagnetic stripes (DFFS) as well as A- and C-type diagonal filled antiferromagnetic stripes (ADFAS, CDFAS), which allows us to compare ferromagnetic with antiferromagnetic coupling both within the NiO planes (intraplane) and between adjacent planes (interplane).

The electronic states at the Fermi energy are expected to grow out of the Ni 3d and O 2p orbitals, due to Ni-O bonding. This is confirmed by fig. 2, which shows the Ni and O partial densities of states (DOS) resulting from a spin-degenerate LDA+ $U$  calculation. Contributions of La and Sr states in the energy interval of fig. 2 are very small and play no role for the further discussion. Here, and in the following LDA+ $U$  calculations, local interactions are assumed for both the  $\text{Ni}^{2+}$  and  $\text{Ni}^{3+}$  sites. For the onsite Coulomb interaction we choose a value of  $U = 8\text{ eV}$  and for the Hund's coupling a value of  $J_H = 0.8\text{ eV}$  [28, 29]. In fig. 2 we identify two groups of electronic bands, the first extending from about  $-8\text{ eV}$  to  $-1.6\text{ eV}$ , with respect to the Fermi energy. The second, being separated from the first group by an energy gap of  $0.7\text{ eV}$ , starts at about  $-1.9\text{ eV}$  and extends far beyond the Fermi level. Whereas O 2p contributions concentrate in the low energy group of bands, the DOS at higher energy is dominated by the Ni 3d states. In particular, a pronounced DOS structure is evident at the Fermi energy, which points towards an instability against magnetic ordering.

Introduction of the spin-polarization has serious effects on the DOS of the magnetic Ni atoms. In figs. 3 and 4 we address the spin-polarized partial Ni 3d DOS, separated into contributions from the four crystallographically inequivalent Ni sites, for two possible antiferromagnetic spin patterns of  $\text{La}_{5/3}\text{Sr}_{1/3}\text{NiO}_4$ . The magnetic structure of the ADFAS phase (fig. 3) is based on a ferromagnetic ar-

angement of domain walls and magnetic domains, an intraplane ferromagnet, and antiferromagnetic coupling between adjacent planes. On the contrary, in the case of the CDFAS (fig. 4) the diagonal stripes are ordered antiferromagnetically within the NiO planes, as depicted in fig. 1, whereas the coupling is ferromagnetic along the perpendicular  $c$ -axis. For both antiferromagnetic spin patterns, the DOS shows a broad structure of occupied Ni 3d states, and a finite number of states at the Fermi energy. Lacking of an insulating band gap, however, contradicts an experimental gap of  $0.26\text{ eV}$  [19, 20]. In figs. 3 and 4 we find broad spin-minority bands extending far beyond the Fermi level. For the ADFAS phase the same applies to the spin-majority states, while for antiferromagnetic intraplane coupling these states give rise to a much more pronounced structure with a remarkable weight at the Fermi level. In addition, we have tried several other spin patterns in order to obtain an insulating state, but without any success. In each case, the system appeared to be far from opening a band gap. Furthermore, we have investigated whether a local interaction on the oxygen sites has to be taken into account. While the total energy in fact slightly decreases for reasonable values of  $U$  and  $J_H$ , the DOS shape changes only marginally near the Fermi level. In a recent LDA+ $U$  study on  $\text{La}_{5/3}\text{Sr}_{1/3}\text{NiO}_4$ , Yamamoto *et al.* [30] have found an insulating solution with an energy gap of  $0.11\text{ eV}$ . However, in contrast to our calculations, their data rely on a spin pattern with antiferromagnetic ordering along the diagonal stripes.

We next address the stability of the spin patterns under consideration. According to table 2, all magnetic solutions are lower in energy than the paramagnetic phase, already for  $U = 0$ . In particular, the DFSF and ADFAS phases turn out to be almost degenerate, both revealing an energy gain of  $5.8\text{ mRyd}$  per Ni atom as compared to the non-

	DFFS	ADFAS	CDFAS	ADFAS, LDA+ $U$	CDFAS, LDA+ $U$
intraplane coupling	fe	fe	af	fe	af
interplane coupling	fe	af	fe	af	fe
magn. moment Ni1 ( $\mu_B$ )	0.72	0.66	1.14	1.66	1.73
magn. moment Ni2 ( $\mu_B$ )	0.71	-0.71	1.10	-1.53	1.63
magn. moment Ni3 ( $\mu_B$ )	0.77	0.72	-1.02	1.68	-1.60
magn. moment Ni4 ( $\mu_B$ )	0.78	-0.78	-0.89	-1.64	-1.55
total energy gain (mRyd)	5.8	5.8	87	152	143

Table 2: Ni magnetic moments and total energy gain (per Ni atom) with respect to non-magnetic calculations. Columns 1 to 3 refer to pure GGA calculations, whereas columns 4 to 6 give the corresponding LDA+ $U$  values. The LDA+ $U$  results are based on the parameters  $U = 8$  eV and  $J=0.8$  eV.

magnetic solution. Because these patterns only differ by their spin arrangement along the  $c$ -axis, we conclude that the magnetic interlayer coupling is very weak. Turning to the comparison of the ADFAS and CDFAS configurations, we obtain that the latter has a substantially lower energy than the former (6.7 mRyd per Ni atom). This energy gain can safely be attributed to the intraplane magnetic coupling, due to the nearly vanishing interplane interaction, as mentioned above. Remarkably, the evaluation of the local magnetic moments self-consistently influences the various hopping matrix elements and crystal fields involved in the calculation. It therefore is unlikely to design a realistic model without accounting for this self-consistency. Nevertheless, a large number of calculations for the two-band Hubbard model clearly point at competing phases, see [31, 32] and the references therein.

Regarding the magnetic moments, we find comparable amplitudes for all Ni sites, independent of the magnetic structure. Remarkably, even in the case of the DFFS configuration the magnetic moments show a strong tendency to stripe formation. Their values increase substantially in the CDFAS phase, see table 2, resulting in a lower energy. Note that the total magnetic moment is finite in one unit cell, amounting to  $0.35 \mu_B$  per Ni site. Nevertheless, the moment is expected to vanish if the supercell would be doubled in the  $c$ -direction. Since the interlayer coupling is almost negligible, the result of such a calculation would be closely related to the present data, yet producing a vanishing total magnetization. Our calculation thus captures all relevant features of the CDFAS phase. Moreover, a solution with vanishing intraplane magnetic moment could not be obtained, and therefore is likely to be either higher in energy or not to exist.

Concerning the magnetic state of the Ni ions, we find a superposition of  $S_z = 1/2$  ( $\text{Ni}^{3+}$ -like) with  $S_z = 0$  and  $S_z = 1$  states ( $\text{Ni}^{2+}$ -like, one electron in each  $e_g$  orbital with parallel/antiparallel spin), whereas states involving doubly occupied orbitals are suppressed [33]. When the onsite electron-electron interaction is included ( $U = 8$  eV,  $J_H = 0.8$  eV), the local magnetic moments increase significantly, to about  $1.6 \mu_B$  in both antiferromagnetic phases. This modification arises from a combined effect of  $U$  and

$J_H$ , as suggested by model calculations [33]. However, the increase is amplified in the ADFAS phase as compared to the CDFAS phase, favoring the former by 9 mRyd per Ni atom. Thus, the energy order of the antiferromagnetic patterns is inverted due to the onsite interaction, hence no longer reflecting the experimental situation. This fact indicates strong interplay between the magnetic structure, the onsite Coulomb interaction, and the energetical sequence of the magnetic phases. We have verified that the latter is not sensitive to (i) the exact values of  $U$  and  $J_H$ , in a reasonable range compared to experimental data, and (ii) the inclusion of a local interaction on the O sites. Combining the above with the absence of an insulating ground state in our band structure calculation leaves little room for an explanation of the deviation from the experimental observation: one appealing scenario is provided by the fact that the final determination of the crystal structure, in particular the positional parameters of all atoms, has not been performed so far. The structural estimates used for the atomic positions can be inadequate, suggesting to perform a structure optimization. Up to now, however, a realistic structure optimization could not be realized due to a large number of lattice degrees of freedom. As structural relaxation is expected to be very sizeable for  $\text{NiO}_6$  octahedra, modification of the Ni-O bonding could easily alter the electronic structure in the vicinity of the Fermi energy, such that an insulating gap arises. Of course, this might correct the energy sequence of the spin patterns.

In summary, we have presented a series of spin-resolved electronic structure calculations for the striped nickelate  $\text{La}_{5/3}\text{Sr}_{1/3}\text{NiO}_4$ , including onsite Coulomb interaction. In contrast to experimental findings, the LDA+ $U$  approach results in A-type diagonal filled antiferromagnetic stripes, while in the pure GGA scheme C-type diagonal filled antiferromagnetic stripes are favored. Our results indicate that accordance with the experimental situation calls for further determination of the structural parameters, since  $\text{NiO}_6$  octahedra are known to be subject to strong structural distortions in many cases. We expect that the same applies to all commensurate doping levels.

\* \* \*

We thank V. Eyert, T. Kopp, and M. Raczkowski for helpful discussions, and acknowledge financial support by the Deutsche Forschungsgemeinschaft (SFB 484) and the Bayerisch-Französische Hochschulzentrum.

## REFERENCES

- [1] J.M. TRANQUADA, J.D. AXE, N. ICHIKAWA, Y. NAKAMURA, S. UCHIDA and B. NACHUMI, *Phys. Rev. B*, **54** (1996) 7489.
- [2] P. ABBAMONTE, A. RUSYDI, S. SMADICI, G.D. GU, G.A. SAWATZKY, and D.L. FENG, *Nature Physics*, **1** (2005) 155.
- [3] Y. KOHSAKA, C. TAYLOR, K. FUJITA, A. SCHMIDT, C. LUPIEN, T. HANAGURI, M. AZUMA, M. TAKANO, H. EISAKI, H. TAKAGI, S. UCHIDA and J.C. DAVIS, *Science*, **315** (2007) 1380.
- [4] Q. LI, M. HÜCKER, G.D. GU, A.M. TSVELIK, and J.M. TRANQUADA, *Phys. Rev. Lett.*, **99** (2007) 067001.
- [5] S.-H. LEE AND S-W. CHEONG, *Phys. Rev. Lett.*, **79** (1997) 2514.
- [6] H. YOSHIZAWA, T. KAKESHITA, R. KAJIMOTO, T. TANABE, T. KATSUFUJI and Y. TOKURA, *Phys. Rev. B*, **61** (2000) R854.
- [7] S.-H. LEE, J.M. TRANQUADA, K. YAMADA, D.J. BUTTREY, Q. LI and S.-W. CHEONG, *Phys. Rev. Lett.*, **88** (2002) 126401.
- [8] P.G. FREEMAN, A.T. BOOTHROYD, D. PRABHAKARAN, D. GONZÁLEZ and M. ENDERLE, *Phys. Rev. B*, **66** (2002) 212405.
- [9] M. HÜCKER, M. VON ZIMMERMANN, R. KLINGELER, S. KIELE, J. GECK, S.N. BAKEHE, J.Z. ZHANG, J.P. HILL, A. REVCOLEVSCHI, D.J. BUTTREY, B. BÜCHNER, and J.M. TRANQUADA, *Phys. Rev. B*, **74** (2006) 085112.
- [10] E. DAGOTTO, *Nanoscale Phase Separation and Colossal Magnetoresistance* (Springer Series in Solid State Sciences Vol. 136, Springer-Verlag, Heidelberg) 2003.
- [11] T. KIMURA, K. HATSUDA, Y. UENO, R. KAJIMOTO, H. MOCHIZUKI, H. YOSHIZAWA, T. NAGAI, Y. MATSUI, A. YAMAZAKI and Y. TOKURA, *Phys. Rev. B*, **65** (2002) 020407(R).
- [12] S. LAROCHELLE, A. MEHTA, L. LU, P.K. MANG, O.P. VAJK, N. KANEKO, J.W. LYNN, L. ZHOU and M. GREVEN, *Phys. Rev. B*, **71** (2005) 024435.
- [13] J. ZAAENEN and A.M. OLEŚ, *Ann. Phys. (Leipzig)*, **5** (1996) 224.
- [14] M. RACZKOWSKI, R. FRÉSARD, and A.M. OLEŚ, *phys. stat. sol. (b)*, **244** (2007) 2521.
- [15] M. RACZKOWSKI, R. FRÉSARD, and A.M. OLEŚ, *Europhys. Lett.*, **76** (2006) 128.
- [16] M. RACZKOWSKI, R. FRÉSARD and A.M. OLEŚ, *Phys. Rev. B*, **73** (2006) 094429.
- [17] J. ZAAENEN and P.B. LITTLEWOOD, *Phys. Rev. B*, **50** (1994) 7222.
- [18] A.P. RAMIREZ, P.L. GAMMEL, S.-W. CHEONG, D.J. BISHOP and P. CHANDRA, *Phys. Rev. Lett.*, **76** (1996) 447.
- [19] S.-W. CHEONG, H.Y. HWANG, C.H. CHEN, B. BATLOGG, L.W. RUPP, JR. and S.A. CARTER, *Phys. Rev. B*, **49** (1994) 7088.
- [20] T. KATSUFUJI, T. TANABE, T. ISHIKAWA, Y. FUKUDA, T. ARIMA and Y. TOKURA, *Phys. Rev. B*, **54** (1996) R14230.
- [21] Y. TAKEDA, R. KANNO, M. SAKANO, O. YAKAMOTO, M. TAKANO, Y. BANDO, H. AKINAGA, K. TAKITA, and J.B. GOODENOUGH, *Mat. Res. Bull.*, **25** (1990) 293.
- [22] N. NGUYEN, F. STUDER, and B. RAVEAU, *J. Phys. Chem. Solids*, **44** (1983) 389.
- [23] P. BLAHA, K. SCHWARZ, G. MADSEN, D. KVASICKA, and J. LUITZ, *Wien2k: An augmented plane wave + local orbitals program for calculating crystal properties* (Vienna University of Technology) 2001.
- [24] U. SCHWINGENSCHLÖGL and C. SCHUSTER, *Europhys. Lett.*, **79** (2007) 27003; *Eur. Phys. J. B*, **55** (2007) 43; *Appl. Phys. Lett.*, **90** (2007) 192502; *Europhys. Lett.*, **77** (2007) 37007.
- [25] J.P. PERDEW, S. BURKE, and M. ERNZERHOF, *Phys. Rev. Lett.*, **77** (1996) 3865.
- [26] V.I. ANISIMOV, I.V. SOLOVYEV, M.A. KOROTIN, M.T. CZYZYK, and G.A. SAWATZKY, *Phys. Rev. B*, **48** (1993) 16929.
- [27] A.I. LIECHTENSTEIN, V.I. ANISIMOV, and J. ZAAENEN, *Phys. Rev. B*, **52** (1995) R5467.
- [28] V.I. ANISIMOV and O. GUNNARSSON, *Phys. Rev. B*, **43** (1991) 7579.
- [29] V.I. ANISIMOV, D. BUKHVALOV, and T.M. RICE, *Phys. Rev. B*, **59** (1999) 7901.
- [30] S. YAMAMOTO, Y. HATSUGAI, and T. FUJIWARA, *Phys. Rev. B*, **76** (2007) 165114.
- [31] R. FRÉSARD, M. RACZKOWSKI, and A.M. OLEŚ, *phys. stat. sol. (b)*, **242** (2005) 370.
- [32] M. RACZKOWSKI, R. FRÉSARD, and A.M. OLEŚ, *J. Phys.: Condens. Matter*, **18** (2006) 7449.
- [33] R. FRÉSARD and M. LAMBOLEY, *J. Low Temp. Phys.*, **126** (2002) 1091.